

CHEMISTRY

A European Journal

A Journal of



Accepted Article

Title: Paramagnetic Lanthanide NMR Probes Signalling Changes in Zinc Concentration by Emission and Chemical Shift: A Proof of Concept Study

Authors: David Parker, Alice C. Harnden, and Andrei S. Batsanov

This manuscript has been accepted after peer review and appears as an Accepted Article online prior to editing, proofing, and formal publication of the final Version of Record (VoR). This work is currently citable by using the Digital Object Identifier (DOI) given below. The VoR will be published online in Early View as soon as possible and may be different to this Accepted Article as a result of editing. Readers should obtain the VoR from the journal website shown below when it is published to ensure accuracy of information. The authors are responsible for the content of this Accepted Article.

To be cited as: *Chem. Eur. J.* 10.1002/chem.201900609

Link to VoR: <http://dx.doi.org/10.1002/chem.201900609>

Supported by
ACES

WILEY-VCH

Paramagnetic Lanthanide NMR Probes Signalling Changes in Zinc Concentration by Emission and Chemical Shift : A Proof of Concept Study

Alice C. Harnden, Andrei S. Batsanov and David Parker *

Department of Chemistry, Durham University, South Road, Durham DH1 3LE, UK

A zinc-selective probe, based on a set of rare earth complexes of a modified DO3A macrocyclic ligand incorporating a tris-pyridylamine (TPA) moiety has been structurally characterised in solution and in the solid-state. One pyridine group possesses a *tert*-butyl substituent to serve as an NMR reporter group. The mono-capped square-antiprismatic Dy complex has a long bond (2.83Å) to an apical N atom (pK_a 5.70 Eu) and binds to one water molecule on zinc binding. Zinc binding is reversible, and involves all of the exocyclic ligand N donors; it is signalled by large (ratiometric) changes in Eu emission intensity, and by dramatic changes in the size (>50 ppm) and sign of the chemical shift of the paramagnetically shifted ^tBu resonances in Tb, Dy and Tm complexes. Slow trans-metallation was observed, leading to formation of an unusual di-zinc species in which one zinc ion is 7-coordinate and the other is six-coordinate.

The Zn²⁺ ion is the second most abundant transition metal ion in the body. Most of this is tightly bound within metalloproteins, where zinc plays a key role in enzymatic catalysis and structural organisation. However, it has also been found to be an important signalling ion, and relatively high concentrations of free Zn²⁺ (μM to mM range) can be present in the extracellular matrix of several organs, notably the pancreas and prostate glands.¹ Disruption of normal Zn²⁺ homeostasis has been associated with many diseases, such as diabetes and prostate cancer. Elevated levels of zinc in the brain have also been linked to certain neurodegenerative disorders, including Alzheimer's disease.

The abundance and importance of Zn^{2+} in biology has led to the development of many chemical sensors, most commonly based on fluorescence detection.^{2,3} Typically these sensors are small molecular probes containing a fluorescent reporting unit appended with selective Zn^{2+} binding groups, such as the cell-permeable emissive probe Zinpyr-1 described by Lippard and Tsien.⁴ It is sensitive in the mid-nanomolar range, as a second ion is reversibly bound. The most frequently used chelating moieties incorporated into Zn^{2+} sensors are tris- and bis(2-pyridylmethyl)amine, also known as tri and dipicolylamine (TPA/DPA). The ligands TPA and DPA form relatively stable complex ML complexes with Zn^{2+} ($\log K_{\text{ZnL}} = 11.0$ and 6.8 respectively)⁵ with no measurable affinity for the abundant divalent cations Ca^{2+} and Mg^{2+} .⁶

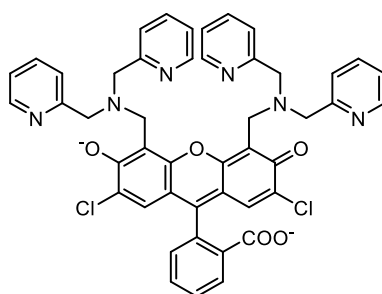


Figure 1 Structure of Zinpyr-1, where successive Zn^{2+} binding constants are $\log K = 8.3$ and 7.1 (298K)

Zn^{2+} sensors for magnetic resonance studies have also been designed. Initially, they were Gd^{3+} -based complexes with proton relaxivity values that varied as a function of Zn^{2+} concentration.^{7,8}

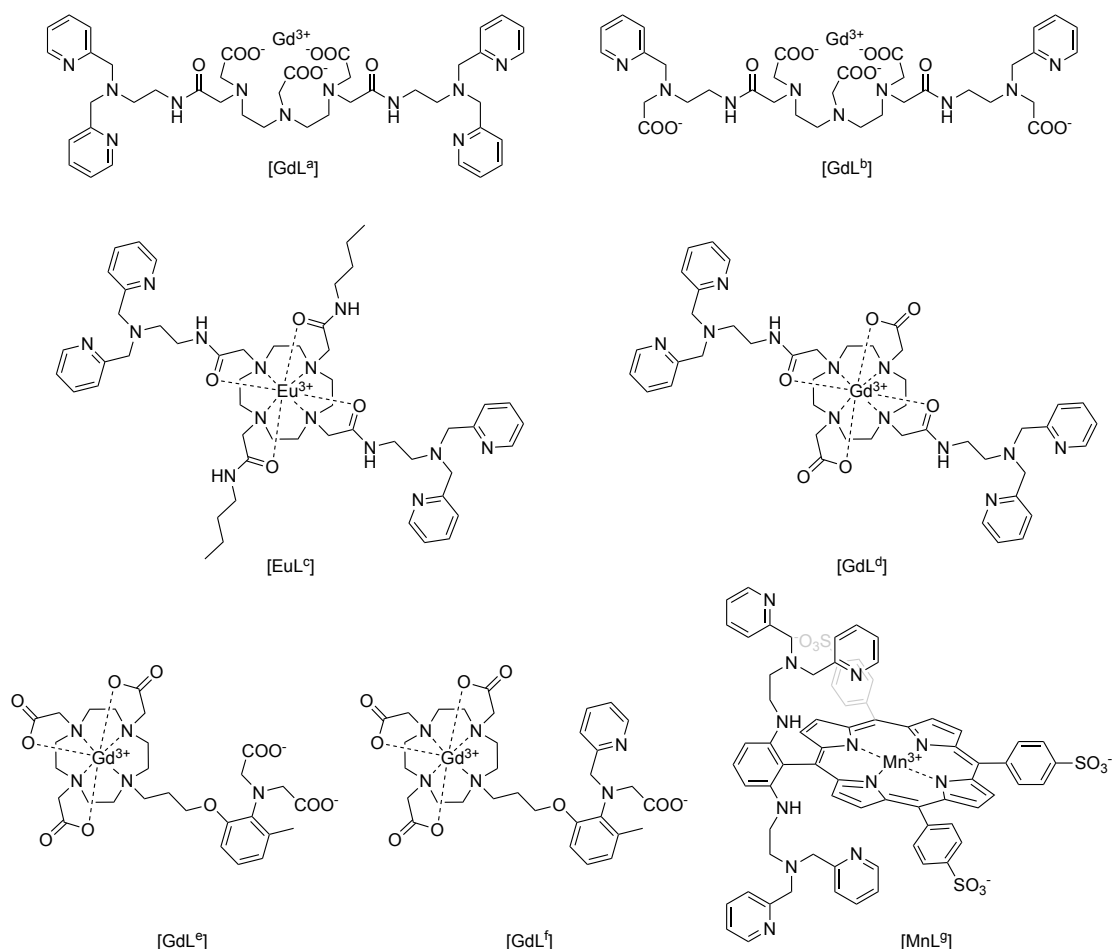


Figure 2 Representative examples of magnetic resonance Zn^{2+} probes.

Nagano and co-workers designed the first Zn^{2+} sensing MRI probe, based on a Gd-DTPA backbone appended with two DPA moieties, [GdL^a], (Figure 2).⁹ Upon addition of up to 1 equivalent of Zn^{2+} , the relaxivity of the complex decreased by 33%. In the resulting 1:1 complex, the Zn^{2+} ion is coordinated by each DPA unit. The hydrophobic pyridine moieties sterically inhibit the second sphere of hydration around the Gd³⁺ ion, causing the decrease in relaxivity. However, this change is reversed upon the further addition of Zn^{2+} as a less sterically demanding 2:1 complex forms at higher concentrations. The replacement of one pyridine unit of each DPA moiety by a carboxylate group, [GdL^b] (Figure 2) circumvented this problem as the 2:1 complex was no longer favoured, meaning the 30% relaxivity decrease was maintained, even after addition of excess Zn^{2+} .¹⁰

Sherry and co-workers developed a Eu³⁺ PARACEST probe for the selective signalling of Zn^{2+} , based upon a cyclen-tetraamide macrocycle appended with two DPA moieties, [EuL^c] (Figure 2).¹¹ Following addition of Zn^{2+} , the CEST

magnitude of the exchanging inner sphere water molecule decreased and this behaviour was attributed to a faster water exchange rate. Phantom imaging experiments demonstrated selectivity against Mg^{2+} and Ca^{2+} . However, the loss of the CEST signal was also found to be pH dependent, and there is a marked inherent temperature dependence of the chemical shift of the proton resonances.

The PARACEST probe, **[EuL^c]**, was modified to create a Gd^{3+} -based relaxivity probe, in which two of the amides were replaced with carboxylates, **[GdL^d]** (Figure 2).¹² A modest increase (20%) in relaxivity was observed with the addition of Zn^{2+} until 2 equivalents had been added. The increase in relaxivity was suggested to be due to the presence of the Zn^{2+} cation, promoting a faster water exchange rate at the Gd^{3+} ion. When the same addition of Zn^{2+} was performed in the presence of human serum albumin (HSA), a significantly larger increase (165%) in the relaxivity was observed, attributed to an increase in the rotational correlation time for the complex when bound to the large protein. *In vivo* studies demonstrated that the complex could be used to monitor the glucose-stimulated co-release of Zn^{2+} with insulin from pancreatic β -cells.¹³ It was shown that mice on high-fat diets displayed higher contrast enhancement upon injection of glucose and **[GdL^d]**, consistent with pancreatic expansion and concomitant increase in β -cell function. More recently the same complex was investigated for the detection of the release of Zn^{2+} in the prostate.¹⁴

GdDO3A -based Zn^{2+} sensors were also investigated by Meade and co-workers, e.g., **[GdL^e]** and **[GdL^f]** (Figure 2), in which the relaxivity increased upon binding of Zn^{2+} .^{15,16} The aminoacetate groups in **[GdL^e]** were ^{13}C -labeled providing direct evidence of carboxylate binding to the paramagnetic centre, in the absence of Zn^{2+} . In the free complex, the Gd^{3+} ion is coordinatively saturated with no bound water and a relatively low relaxivity value. Upon addition of Zn^{2+} , the relaxivity increased by over 100%.

Lippard and co-workers designed a dual-function Mn^{2+} -based probe for MRI and fluorescence, **[MnL^g]** (Figure 2).¹⁷ The fluorescence and relaxivity of the porphyrin complex was modulated by the presence of Zn^{2+} . The probe showed a 24% decrease in relaxivity upon addition of one equivalent of Zn^{2+} and the near

infrared (NIR) fluorescence emission intensity increased by a factor of ten. The water-soluble porphyrin probe was able to permeate cell membranes and MR experiments demonstrated that the probe could induce lower relaxivity values in cells incubated with Zn^{2+} . The contrast agent was shown to penetrate effectively and stain cells *in vivo* by a series of experiments with intracranially injected rats.¹⁸ However, in the regions of the brain with known higher concentrations of Zn^{2+} , the contrast enhancement was found to be greater than in regions with lower concentration of Zn^{2+} , the opposite of the dependence found in the *in vitro* and cellular experiments. Evidently, calibration is an issue yet to be resolved.

Each of the MRI contrast agents described above rely on indirect methods of detection. The relaxation time of the bulk water signal is measured to assess the Zn^{2+} concentration. It is not possible, however, to determine the Zn^{2+} concentration without knowing the concentration of the probe in each voxel studied. Local concentrations cannot be known *in vivo* without additional efforts to estimate contrast agent concentration. The use of PARASHIFT probes¹⁹⁻²¹ provides an opportunity to remove this limitation, as the probe itself reports the presence of Zn^{2+} by modulation of a concentration independent parameter, i.e. the chemical shift of a probe reporter resonance, whose shift is a function of $[\text{Zn}^{2+}]$. Up till now, studies of such probes have examined their use to report temperature and pH, with limits of detection of the order of 10 to 20 μM (7T, 310K) reported *in vivo*.¹⁹⁻²¹ In this work, we seek to develop a proof of principle using a PARASHIFT system that can report the change in zinc ion concentration.

A Eu^{3+} -based Zn^{2+} luminescence sensor has been reported by Pope, which contained a pyridine group appended with a DPA moiety, based on a D03A macrocycle, **[EuL^h]** (Figure 3).²² Following addition of 1 equivalent of ZnCl_2 , the observed europium luminescence emission varied. It was shown that a 1:1 complex formed with Zn^{2+} , and the spectral changes that occurred were interpreted in terms of modulation of the Eu^{3+} coordination environment, as the proximal pyridine group dissociated to be replaced by a water molecule.

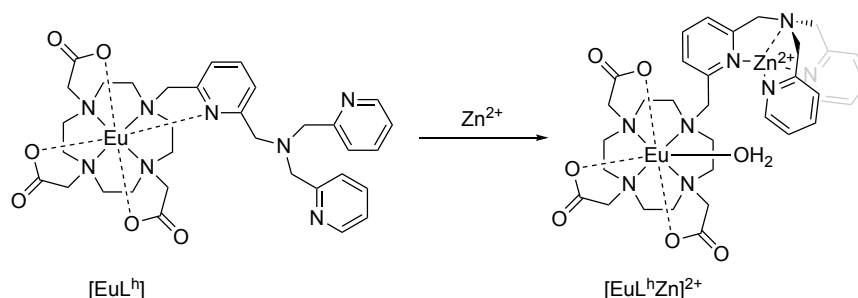
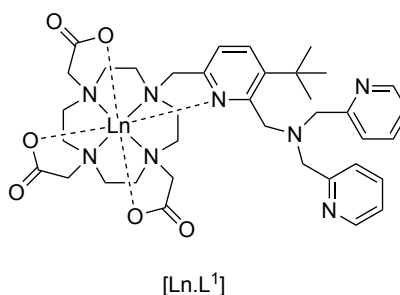


Figure 3 Structure of a luminescent Eu^{3+} -based Zn^{2+} probe as originally proposed ²² showing the change in Eu coordination upon Zn^{2+} binding; a water molecule is bound to the Zn ion.

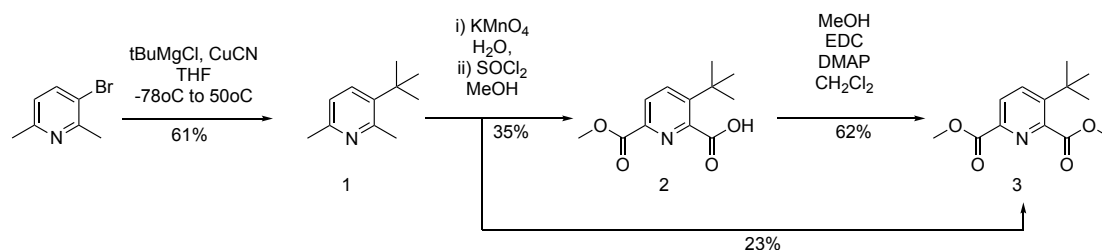
Accordingly, we set out to modify the ligand structure in **[EuL^h]** by adding a *tert*-butyl reporter group adjacent to the Zn^{2+} binding moiety, thereby creating a metal ion responsive PARASHIFT probe, **[Ln.L¹]**. It was reasoned that the large change in both the ligand field, geometric coordinates and magnetic susceptibility anisotropy that occurs on zinc binding would lead to a significant change in the chemical shift of the proximate *t*-butyl resonance.



Results and Discussion

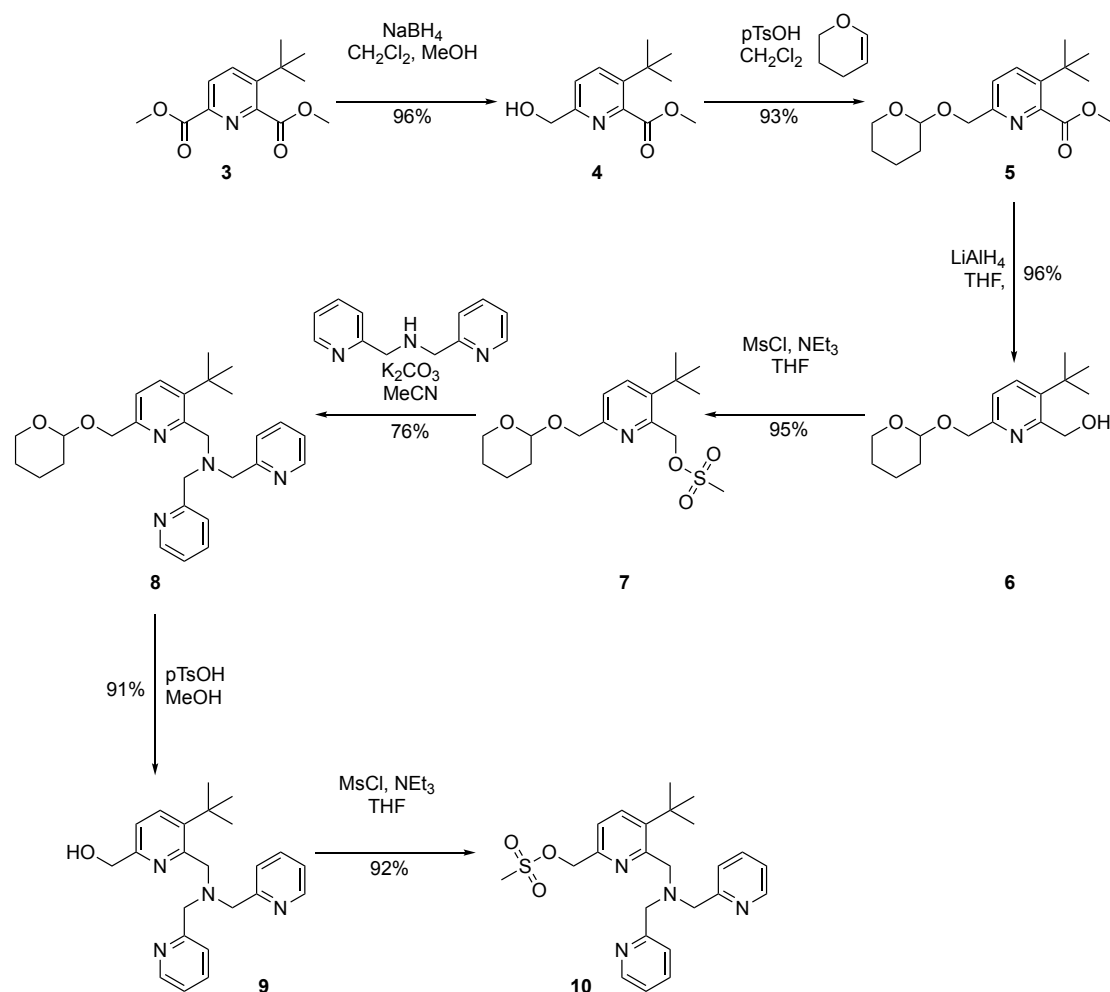
The synthesis of **L¹** (Schemes 1-2) was undertaken, using adaptations of literature methodology. Reaction of 3-bromo-2,6-dimethylpyridine with *tert*-butyl magnesium chloride, was promoted by the presence of cuprous cyanide and required heating to 50°C overnight in THF, to ensure formation of the 3-substituted derivative, **1**. Oxidation with KMnO_4 gave the crude dicarboxylate salt that was reacted successively with thionyl chloride and methanol to yield a mixture of the esters **2** and **3**. ^1H NMR analysis revealed two major products and inspection of the 2D ^1H - ^{13}C HMBC NMR spectrum showed that the mono-ester, **2**, was the 6-carboxy isomer. Rapid formation of the di-ester is sterically inhibited by the proximate *tert*-butyl group. Indeed, separate esterification under the same conditions with the isolated monoester product, **2**, gave no reaction.

However, a Steglich esterification reaction using EDC and DMAP as the acyl transfer catalyst yielded the di-ester, **3**.



Scheme 1

Selective reduction of the diester, **3**, was achieved using sodium borohydride at 0°C. NMR analysis of the reaction mixture confirmed the presence of one product, consistent with regioselective reduction of the less sterically hindered ester group, in near quantitative yield after chromatography. Two dimensional NOESY NMR spectroscopic experiments verified the constitution of this regioisomer: through-space correlations were found between the *tert*-butyl resonance and the ester methyl group, corroborated by the presence of a cross peak between the pyridine H⁵ proton and the hydroxymethyl methylene protons, (Fig S1)..Protection of the alcohol was achieved by reaction of **4** with 3,4-dihydro-2H-pyran in the presence of *p*-toluenesulfonic acid to yield the tetrahydropyranyl ether **5** (Scheme 2). The hindered ester group was reduced cleanly with lithium aluminium hydride at 0°C to give the alcohol **6**. Conversion to the mesylate, **7**, was undertaken using methanesulfonyl chloride and triethylamine, prior to mono-alkylation of dipicolylamine. Purification of the tertiary amine, **8**, used column chromatography on alumina. The THP ether was hydrolysed with *p*-toluenesulfonic acid in methanol to yield the alcohol, **9**, which was subsequently converted to the mesylate ester, **10**.



Scheme 2

Alkylation of the *tris-t*-butyl ester of DO3A (DO3A = 1,4,7-*tris*(carboxymethyl)-1,4,17,10-tetraazacyclododecane) with **10** in MeCN afforded the tertiary amine, and after treatment with TFA, the complexes of L^1 with Eu, Tb, Dy, Y, Tm and Yb were prepared by reaction with the appropriate LnCl_3 salt at pH 5.5. Each complex was purified by reverse phase HPLC.

Hydration State and Structural Analysis of $[\text{Dy} \cdot L^1]$

The inner sphere hydration state, q for the europium and terbium complexes was calculated by measuring the luminescence lifetimes of $[\text{Eu}L^1]$ and $[\text{Tb}L^1]$ in both H_2O and D_2O , (Table 1), and applying established equations to estimate the lanthanide hydration state.²³

Table 1 Luminescence lifetime measurements of [EuL¹] and [TbL¹] (295 K, λ_{ex} = 276 nm, pH/pD = 7.3).

Ln	$\tau_{\text{D}_2\text{O}}$ (ms)	$\tau_{\text{H}_2\text{O}}$ (ms)	q^{23}
Eu	1.61	1.15	0
Tb	2.78	2.55	0

A q value of zero was calculated from these experimental data,²³ in agreement with the results of Pope.²² In order to verify the coordination around the metal ion, the X-ray structure of [Dy.L¹] was carried out. Crystals of [DyL¹] were grown by slow diffusion of diethyl ether into a methanol solution of the complex (Figure 4). The complex crystallised in the centrosymmetric space group $P2_1/c$, with both enantiomers present within the crystal lattice and symmetry related. Hydrogen bonding was present, two of the carbonyl groups serving as H-bond acceptors to two donor solvent methanol molecules. The coordination number of Dy³⁺ in [DyL¹] is 9, with an N₆O₃ environment: the Dy³⁺ ion is coordinated by the four ring nitrogen atoms (N₁₋₄) and the *tert*-butyl substituted pyridine nitrogen atom (N_{5py}) and three anionic oxygen atoms (O₃) in a SAP geometry (Δ -($\lambda\lambda\lambda\lambda$)). The coordination sphere is completed by the DPA amine nitrogen atom, N₆, which caps the square antiprism.

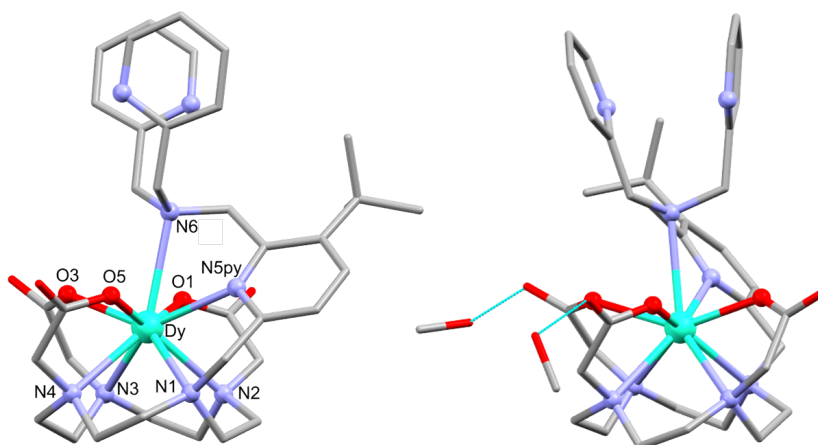


Figure 4 (*left*) Molecular structure of Δ -($\lambda\lambda\lambda\lambda$)-[DyL¹] (120K); (*right*) structure of [DyL¹] showing the hydrogen bonding to solvent methanol, H atoms are omitted for clarity. CCDC 1896075

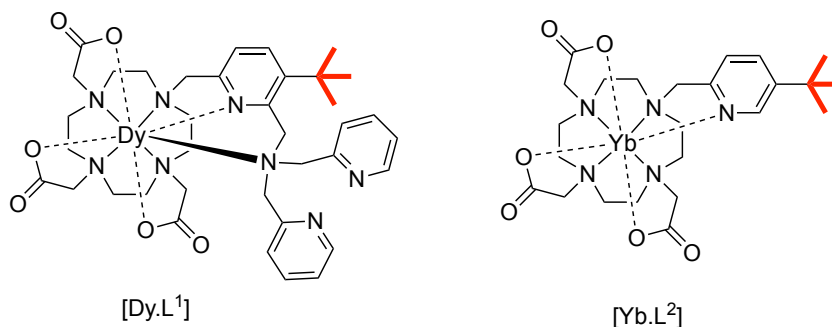
Bond distances between the Dy³⁺ ion and the donors varied (Table 2). The bonds to the neutral nitrogen donors are much longer than those to the anionic

carboxylate oxygen atoms. A long axial bond of 2.83 Å between the lanthanide and the dipicolylamine nitrogen was a notable feature, suggestive of some steric strain in the capping axial site.

Table 2 Bond lengths (Å) for [DyL¹].

bond	bond length (Å)
Dy-N1	2.605(3)
Dy-N2	2.655(3)
Dy-N3	2.654(3)
Dy-N4	2.632(4)
Dy-N5py	2.559(3)
Dy-O1	2.321(3)
Dy-O3	2.266(2)
Dy-O5	2.267(2)
Dy-N6	2.833(3)

The additional axial interaction with the DPA amine nitrogen, (N6), resulted in the metal ion being shifted towards the O₃N antiprism face. In the related carboxylate complex [YbL²], the Yb³⁺ ion is found 1.07 and 1.44 Å from the O₃N and cyclen N₄ bases respectively, (CCDC-1502162)²⁴ whereas in [DyL¹], notwithstanding the impact of the lanthanide contraction and the differing eight coordinate twisted square anti-prismatic coordination geometry of [YbL²], the distances of the Dy³⁺ ion to the O₃N and N₄ bases are 0.78 and 1.61 Å.



pH response of [EuL¹] and [TbL¹]: luminescence studies

To study the pH sensitivity of [LnL¹] a pH titration of the luminescent complex [EuL¹] was carried out. The emission spectrum and emission lifetime were recorded as a function of pH; emission spectra showed an overall decrease in intensity upon lowering pH (Figure 5). A sigmoidal fit, using iterative non-linear least squares methods, plotting the intensity ratio of the largest $\Delta J = 2$ band against the $\Delta J = 0$ band as a function of pH gave a pK_a value of 5.70(05). Similar values were obtained (± 0.06), using the pH variation of the total $\Delta J = 2 / \Delta J = 1$ band intensities. The experimental value of 5.70, suggests that protonation is occurring on the dipicolyl amine nitrogen atom. The observed pK_a value is lower than that reported for the parent trispicolylamine ligand (TPA), for which a value of 6.2 was reported, in accord with the presence of a weak bonding interaction between the Eu³⁺ ion and the N donor atom.^{5b} The sterically bulky *tert*-butyl group and the shielding provided by the three aromatic rings tends to inhibit local solvation, and so will not stabilise the protonated form, i.e. the conjugate acid, as effectively as with less sterically demanding protonated tertiary ammonium ions. The spectral form of [HEu.L¹]⁺ closely resembled that of [Eu.L²], (Fig S2); the latter exists as a 9-coordinate complex, where a water molecule is in the apical site.²⁴

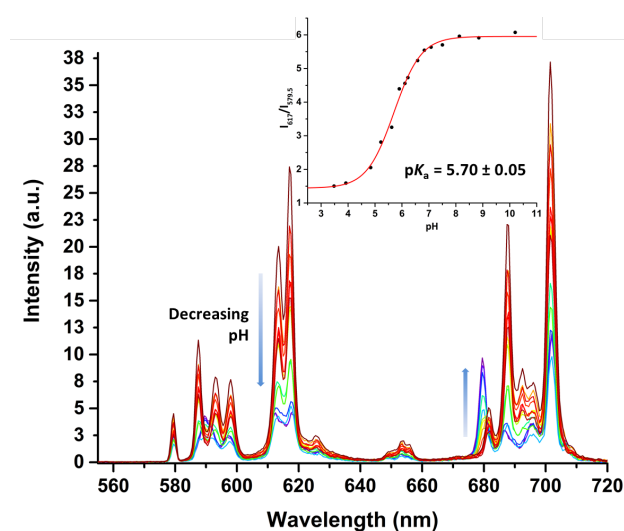


Figure 5 Variation of the emission spectra of [EuL¹] (20 μ M) as a function of pH (H₂O, 295 K, $\lambda_{\text{ex}} = 276$ nm); the inset shows the pH variation of the ratio of emission intensities at 617 nm ($\Delta J = 2$) to 579.5 nm ($\Delta J = 0$).

The luminescence lifetimes observing the $\Delta J = 2$ emission band were also measured in D₂O and H₂O at varying pH (Figure 6). Curiously, whilst the lifetime in H₂O decreased only slightly as the pH fell, the lifetime in D₂O increased by 80%, consistent with a large change in the Eu coordination environment, after taking account of excited state quenching effects due to OH and NH oscillators. Indeed, every emissive Eu species has an intrinsic lifetime that is peculiar to its coordination number and type, once quenching effects associated with vibrational energy transfer to exchangeable OH and NH oscillators have been considered.

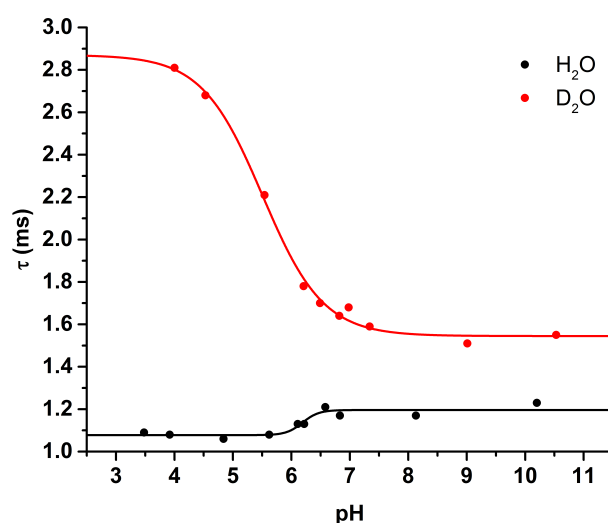


Figure 6 Variation of the lifetime ($\pm 10\%$) of [EuL¹] with pH in H₂O and D₂O (295 K, λ_{ex} 276 nm, λ_{em} 617 nm); here, the values of pH measured refer to the pH meter reading on the x axis scale ($\text{pD} = \text{pH}(\text{meter reading}) + 0.42$).²⁵

The variation of the emission lifetime with pH/pD allowed pK_a values to be estimated, but only the value in D₂O was considered reliable here, owing to the much smaller change in lifetime observed in water and the lower number of useful data points analysed, (Figure 6). The pK_a value in D₂O was estimated to be 5.92(07), higher than the value of 5.70(0.05) found from the emission intensity variation in water. It is known that pK_a values in water and D₂O are normally separated by a value of about +0.4.²⁵

The hydration state of [EuL¹] was also estimated from this data, using the limiting values of the observed lifetimes, i.e. at high and low pH/pD. At high pH q

= 0, and at low pH, the apparent q value was 0.4. Lifetime measurements of $[\text{TbL}^1]$ revealed similar q values at high and low pH/pD, i.e., zero and 0.3 respectively. Such a variation is rationalised by a 9-coordinate structure at high pH, as revealed in the solid-state analysis of $[\text{Dy.L}^1]$, and at low pH the axially bound tertiary amine N (N6, in Figure 4) is protonated and the partial hydration state is explained either by the presence of a weakly bound axial water molecule, (i.e. a long Eu-OH distance), or by the quenching effect of the proximate NH vs ND oscillator of the protonated tertiary amine. It has previously been established that coordinated amine NH oscillators are about twice as effective as bound OH oscillators at quenching Eu^{3+} excited states.²³

Solution NMR studies of $[\text{YL}^1]$

The diamagnetic complex, $[\text{YL}^1]$, was synthesised in order to compare the NMR behaviour with the analogous paramagnetic complexes. ^1H NMR analysis revealed a mixture of broad and sharp resonances within the pyridine aromatic region (Figure 7).

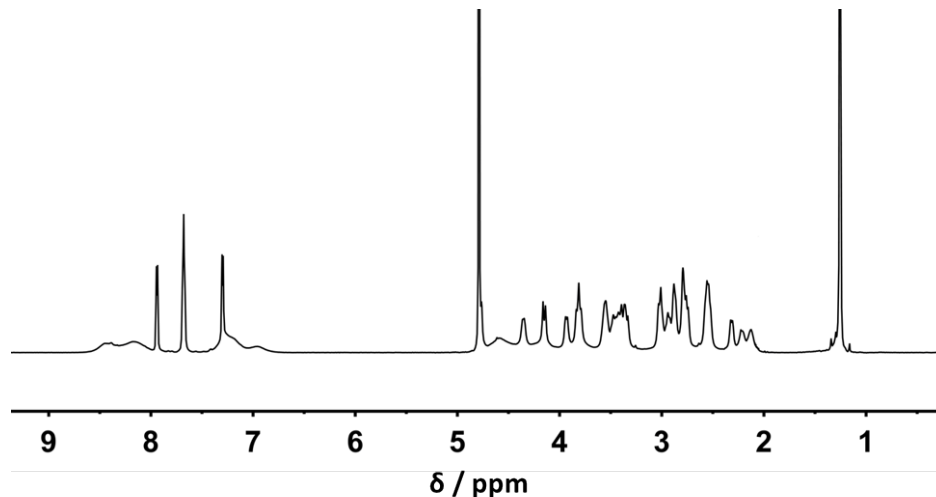


Figure 7 ^1H NMR spectrum of $[\text{YL}^1]$ (D_2O , 16.4 T, 295 K, pD 7.3).

A general assignment was attempted using HSQC, COSY and NOESY 2D NMR spectra. However, no resonances corresponding to the aromatic or picolyl DPA protons could be assigned unequivocally. Whilst the two aromatic proton resonances of the *tert*-butyl pyridine moiety are sharp and readily assigned, several of the aromatic DPA resonances are exchange broadened. Such exchange

broadening is consistent with a chemical exchange process of intermediate rate on the NMR timescale, involving one or more conformers or distinct chemical species associated with the DPA moiety.

Variable temperature NMR was undertaken in an attempt to explore the origins of the broadening of the aromatic resonances (SI: Fig. S3). Upon cooling, multiple resonances appeared within the aromatic region. Above 305 K, these resonances sharpened and coalesced to reveal four distinct picolyl environments. The macrocyclic ring protons also sharpened at lower temperature, but no additional resonances were seen.

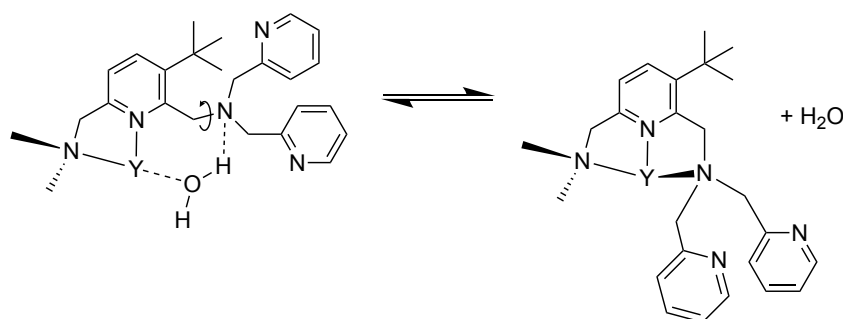


Figure 8 (*right*) Partial structure of the DPA moiety in [Y.L¹] that leads to hindered C-N_{amine} rotation; (*left*) highlighting dissociation of the axially bound M-N bond, postulated to be aided by transient solvolysis of the Y-N bond.

The VT NMR study demonstrates that at temperatures above 285 K, the C-N_{amine} bond (Fig S4 and Figure 8) must be free to rotate sufficiently quickly that the two picolyl rings are rendered equivalent on the NMR timescale. As the temperature decreases, bond rotation slows and the picolyl rings are non-equivalent. A coalescence temperature of 300K was estimated for this chemical exchange process, from which a free energy of activation of 59 kJmol⁻¹ was calculated. Such behaviour can be reasonably associated with the weak interaction between the tertiary amine lone pair and the rare earth ion, in which dissociation of the Eu-N bond, perhaps promoted by solvolysis, has a small energy barrier.

The ¹H NMR spectra of [YL¹] above and below the pK_a were acquired (Figure S3). At low pD (4.5) the aromatic DPA proton resonances were shifted to higher frequency, consistent with protonation of the pyridine N atom. The aromatic

resonances are significantly sharper at low pD, whilst the macrocyclic region is broader. As there are only 6 distinct pyridine environments in acid, the DPA pyridine protons must be equivalent, as observed at higher temperature. The C-N_{amine} bond must have freedom of rotation, on an intermediate NMR timescale. The increased broadness of the macrocyclic ring protons resonances suggests that the rate of exchange between low energy conformations of the ligand backbone is accelerated at low pD. Such behaviour is consistent with the luminescence pK_a data; i.e., the DPA tertiary amine N atom becomes protonated, and the interaction between the metal ion and the amine lone pair is lost. The change from 9- to 8- coordination of the metal ion, results in increased flexibility of the macrocyclic ring arms, to undergo faster cooperative arm rotation, as noted in a large number of dynamic NMR studies of related systems.²⁶

NMR studies of paramagnetic [LnL¹] complexes

The chemical shifts of the *tert*-butyl reporter group of the paramagnetic [LnL¹] complexes were measured in D₂O (Figure 9). In each case, the *tert*-butyl resonance for the Tm³⁺, Tb³⁺ and Dy³⁺ complexes lies well outside the diamagnetic region.

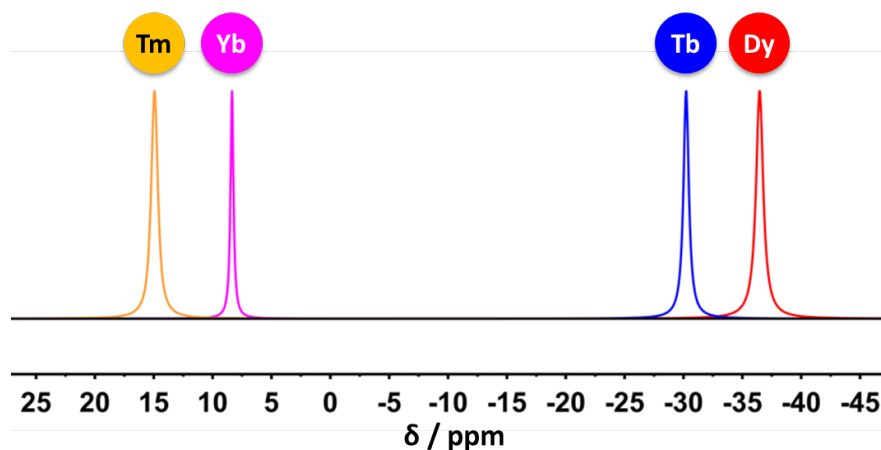


Figure 9 Schematic showing the partial ¹H NMR spectra of the *tert*-butyl resonance of [LnL¹] (D₂O, 4.7 T, 295 K, pD 7.3): Tm (yellow); Yb (magenta); Tb (blue); Dy (red).

In comparison to the analogous carboxylate complex without the Zn²⁺ sensing moiety, [LnL²], the *tert*-butyl pseudocontact chemical shifts are increased. The increase is most significant for the complexes of Dy and Tb. Thus, in [TbL²] and

[DyL²] chemical shifts of -10.6 and -20.1 ppm respectively were observed, ²⁴ compared to -30.2 and -36.5 ppm in **[TbL¹]** and **[DyL¹]**. It has been found that the presence of an axially coordinated water molecule has a significant impact on the paramagnetic shift of lanthanide complexes in structurally related ligands, as the orientation and size of the principal component of the magnetic susceptibility tensor (often the axial component) are sensitive to structural perturbation. The larger chemical shifts in **[LnL¹]** are consistent with the loss of the inner sphere water molecule, as established from the solid-state X-ray structure and the solution lifetime analyses of the Eu³⁺ and Tb³⁺ complexes. Unlike **[LnL²]**, in which two diastereoisomers are observed in solution, only one *tert*-butyl resonance was present for every **[LnL¹]** complex. The weak interaction postulated between the DPA amine and lanthanide(III) ion presumably serves to stabilise the lowest energy conformation and reduces the flexibility of the pendant arms of the 12-N₄ ring.

The longitudinal relaxation rates, R_1 , of the *tert*-butyl resonance of **[LnL¹]** were measured at six different field strengths (Table S1). The rates were similar to those measured with **[LnL²]** ²⁴.

The chemical shift of the reporter *tert*-butyl group was investigated over the temperature range 290 K to 325 K and showed a near linear dependence over this relatively narrow range (Figure 10), wherein **[TbL¹]** and **[DyL¹]**, with the largest paramagnetic shift, have the greatest sensitivities to temperature, of 0.25 and 0.27 ppm/K respectively.

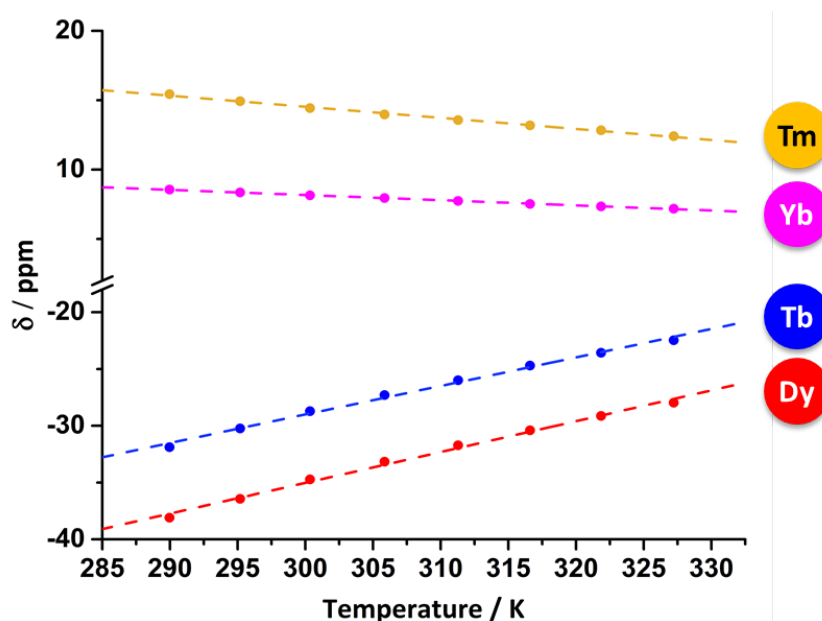


Figure 10 Variation in the chemical shift of the *tert*-butyl resonance of **[LnL¹]** as a function of temperature (D₂O, 11.7 T, pD 7.3): Tm (yellow) $R^2 = 0.996$; Yb (magenta) $R^2 = 0.998$; Tb (blue) $R^2 = 0.994$; Dy (red) $R^2 = 0.995$.

The pH dependence of the chemical shift of **[DyL¹]** was also studied, (Figure 11). From high pD to low pD, the major *tert*-butyl resonance (-36 ppm) broadened and the pseudocontact shift increased (i.e. the chemical shift became more negative), before sharpening (-47 ppm), whilst an additional *tert*-butyl resonance appeared (-60 ppm) and sharpened further as the pD decreased. The presence of two *tert*-butyl resonances, below the pK_a , demonstrates that there are two different forms of the protonated complex that are in slow exchange on the NMR timescale, consistent with the observations with **[HY.L¹]⁺**.

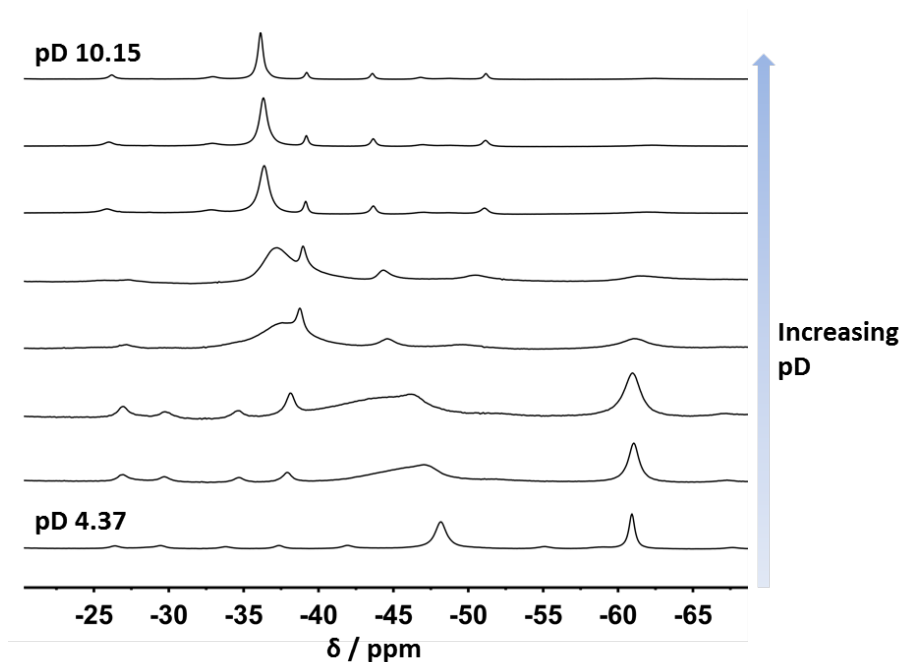


Figure 11 Partial ^1H NMR spectra of **[DyL¹]**, showing the *tert*-butyl resonance, as a function of pD (D_2O , 11.7 T, 295 K).

The longitudinal relaxation rates, R_1 , of the two *tert*-butyl resonances at -47 and -60 ppm at low pD (295 K, 11.7 T) were 164 and 163 s^{-1} respectively, compared to the limiting high pD rate of 181 s^{-1} . The increase in chemical shift, which was also accompanied by an increase in line-width (R_2), indicates that there may be a change in the anisotropy of the pseudocontact shift field. Or, the change may arise from a structural change of the complex that brings the Dy^{3+} centre either closer in space to the *tert*-butyl group, or at a different angle with respect to the main component of the magnetic susceptibility tensor. The longitudinal relaxation rate, R_1 , increases at higher pD, but emission spectral evidence supports the retention of coordination of the proximal pyridine ring, so that the change is unlikely to be the result of a decreased inter-nuclear distance. The loss of the postulated weak interaction of the DPA amine is likely to induce a change in the anisotropy of the pseudo-contact shift field. Variations of the nature of the donor atom in the axial position have previously been shown to have drastic effects on the ligand field and hence the magnetic susceptibility anisotropy in related 8/9 coordinate lanthanide complexes.^{24,27-29}

The presence of two rather broad *tert*-butyl resonances in acid suggests that in the protonated complex there is a chemical exchange process between low

energy conformations of the protonated complex. In the diamagnetic species [YL¹] (Figure 7 and Fig S4) exchange broadening of the macrocyclic resonances was observed at low pD, as a result of the increased flexibility of the macrocyclic backbone. As a result of the greater frequency difference of the two macrocyclic conformations in the paramagnetic complexes two *tert*-butyl resonances are observed at this field.

Zinc binding studies using NMR, MS and emission spectroscopy

The addition of ZnCl₂ to [EuL¹] resulted in a significant emission intensity decrease and changes to spectral form in the $\Delta J = 1, 2$ and 4 manifolds (Figure 12), consistent with a large change in the coordination environment of Eu³⁺.

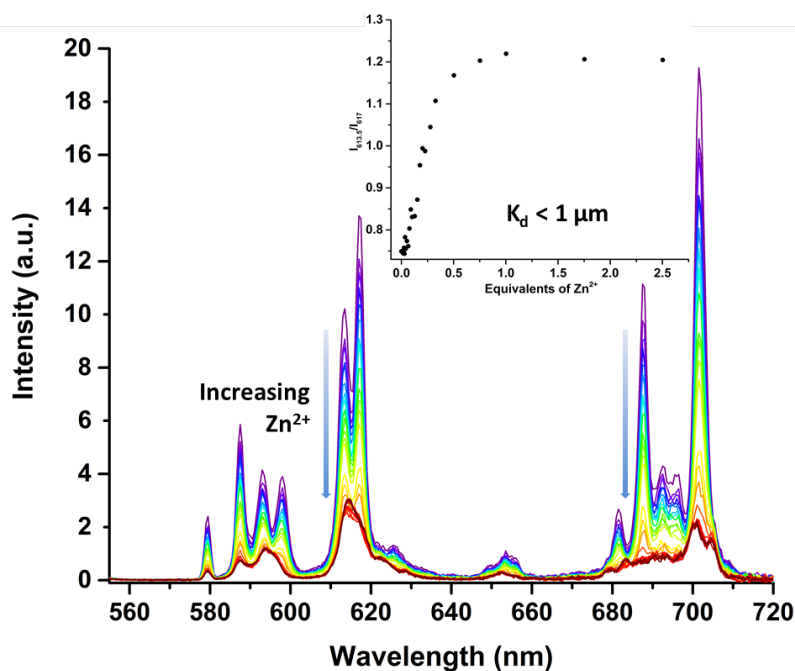


Figure 12 Variation of the emission spectra of [EuL¹] (20 μM) as a function of added equivalents of Zn²⁺. (*Inset*) Intensity ratio of 613.5/617 nm as a function of Zn²⁺ (295 K, H₂O, 0.1 M TRIS, pH/pD = 7.3, λ_{ex} = 276 nm). No spectral changes were observed for addition of up to 10 equivalents of CaCl₂ or MgCl₂

The europium luminescence lifetime was monitored as a function of the number of equivalents of Zn²⁺ added, both in D₂O and H₂O (Table 3, Figure 13). Upon addition of ZnCl₂ the lifetime of the lanthanide excited state increased in D₂O, but decreased in H₂O, as observed on changing pH (Figure 6). The same type of behaviour was observed with [TbL¹], (Table 3). No change in either emission

spectral form or lifetime occurred when up to ten equivalents of CaCl₂ or MgCl₂ were added.

Table 3 Luminescence lifetime measurements ($\pm 10\%$) and complex hydration states ($\pm 20\%$) of **[EuL¹]** and **[TbL¹]**²³ with /without excess Zn²⁺ (295 K, $\lambda_{\text{ex}} = 276$ nm, pH 7.3).

Ln	Zn ²⁺ equivalents	$\tau_{\text{H}_2\text{O}}$ (ms)	$\tau_{\text{D}_2\text{O}}$ (ms)	q
Eu	0	1.15	1.61	0
	5	0.61	1.96	1.1
Tb	0	2.55	2.78	0
	5	1.94	3.19	0.8

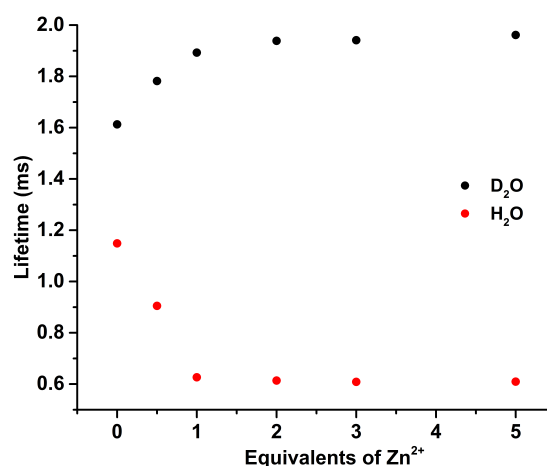
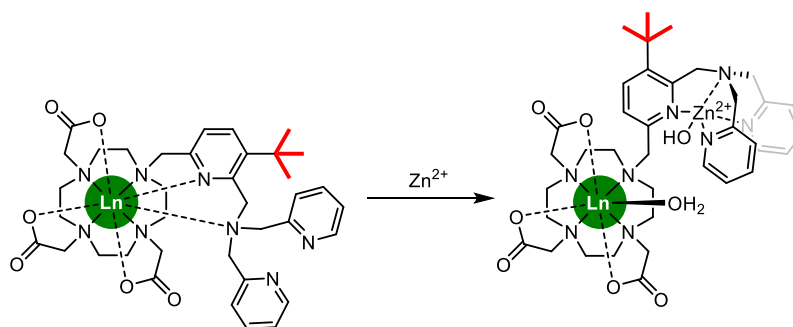


Figure 13 Variation of the lifetime of **[EuL¹]** as a function of equivalents of Zn²⁺ in H₂O and D₂O (295 K, 0.1 M TRIS/TRIS-d₁₁, pH/pD = 7.3, λ_{ex} 276 nm, λ_{em} 617 nm).

The hydration states of the europium and terbium ions following binding of Zn²⁺ were calculated to be $q = 1$ (Table 3).²³ The observed lifetime and emission intensity ratio variations are consistent with limiting 1:1 binding stoichiometry. In the Zn bound complex, the *tert*-butyl pyridine N atom is no longer coordinated to the lanthanide ion, and the zinc ion is coordinated to all three pyridine nitrogen atoms and the tertiary amine N atom (Scheme 3). The coordination at Zn is likely to be completed by a water molecule, as in the Zn complex of TPA.^{5d}



Scheme 3 Proposed structures of **[LnL¹]** without (*left*) and with added Zn^{2+} (*right*). It is assumed that the Zn^{2+} ion will be 5-coordinate and at pH 7.3; Zn coordination is completed by an OH or water molecule.

In order to prove that Zn^{2+} binding is reversible, ligands with a higher affinity for Zn^{2+} (ethylenediaminetetraacetic acid (EDTA) and diethylenetriaminepentaacetic acid (DTPA)) were titrated into a 1:1 solution of **[EuL¹]** and $ZnCl_2$. The titrations revealed restoration of the spectral form of the free complex **[EuL¹]** at high concentrations of the competing ligand, demonstrating that the binding of Zn^{2+} is reversible. The stabilities of the complexes of Zn^{2+} with EDTA and DTPA are $\log K_{ML} = 16.5$ and 18.7 respectively. Binding curves were plotted using the ratio of the intensity integrals for the $\Delta J = 2$ and $\Delta J = 1$ bands. The binding curve constructed for DTPA showed that at a 1:1:1 ratio of Zn^{2+} :**[EuL¹]**:DTPA, almost full restoration of the free complex (~87%) was observed, (Figure 14).

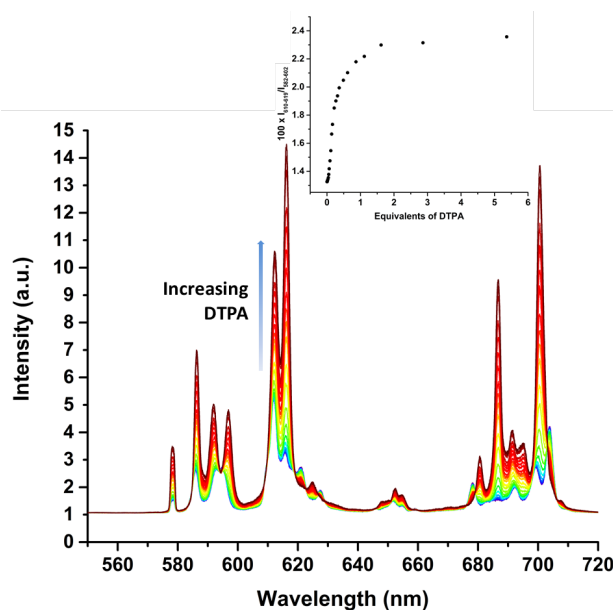


Figure 14 Variation of the emission spectrum of a 1:1 solution of ZnCl_2 ($20 \mu\text{M}$) and $[\text{EuL}^1]$ ($20 \mu\text{M}$) with DTPA concentration. (Inset) Ratio of $\Delta J = 2$ ($I_{610-619 \text{ nm}}$) / $\Delta J = 1$ ($I_{582-610 \text{ nm}}$) as a function of added Zn^{2+} (295 K, H_2O , 0.1 M TRIS, pH 7.3, $\lambda_{\text{ex}} = 276 \text{ nm}$).

Mass spectrometry was used to assess the nature of the Zn^{2+} species with $[\text{LnL}^1]$. Electrospray mass spectrometry experiments were conducted using a 2:1 mixture of $[\text{TbL}^1]$ and ZnCl_2 in H_2O (Figure 15). A 1:2 ratio of $\text{Zn}^{2+}:[\text{TbL}^1]$ was chosen first, to probe the possibility of the presence of a 1:2 ternary complex, as a structurally related system exhibited this stoichiometry.³⁰ The Tb complex was chosen in order to simplify the isotopic pattern, as it has only one stable isotope. The pH of the solution was adjusted to 7.3 with aqueous NaOH in order to recreate the titration conditions, as the presence of buffer suppresses ionisation.

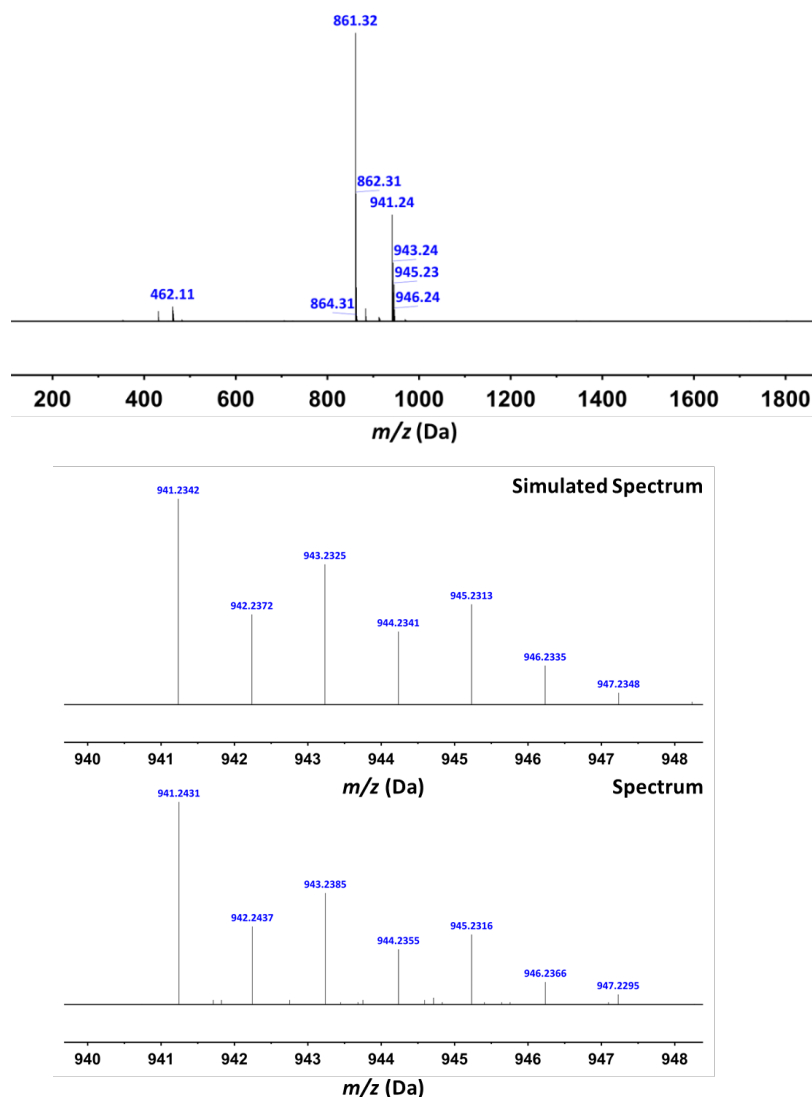


Figure 15 (*upper*) ESI HRMS spectrum of a 1:2 solution of ZnCl_2 and $[\text{TbL}^1]$ in H_2O (pH 7.3); (*lower*) simulated ESI-HRMS (+) spectrum of $\{[\text{TbL}^1]+\text{Zn}+\text{OH}\}^+$ and (*bottom*) observed ESI-HRMS (+) spectrum of $\{[\text{TbL}^1]+\text{Zn}+\text{OH}\}^+$.

The spectrum shows the presence of the protonated complex ($m/z = 861.3$, $\{[\text{TbL}^1]+\text{H}\}^+$), as the major ion and two other species. The doubly charged ion at 462.1 exhibits the distinctive isotope pattern of Zn, and corresponds to $\{[\text{TbL}^1]+\text{Zn}+\text{H}_2\text{O}\}^{2+}$. The ion corresponding to 941.2 is the related singly charged deprotonated complex $\{[\text{TbL}^1]+\text{Zn}+\text{OH}\}^+$ (Figure 15). Typically, adducts still bound to the inner sphere water molecules of lanthanide aqua complexes are not observed in electrospray mass spectrometry. It is therefore reasonable to hypothesise that in solution two water molecules are bound to the complex, one residing on each metal centre, wherein the observed water and the hydroxy

species involve a molecule water and an OH group respectively bound to zinc. It is known that the $[\text{Zn.TPA.H}_2\text{O}]^{2+}$ mono-aqua species possesses a pK_a value of 8.0.^{5d} No species corresponding to any other binding stoichiometry were observed.

The NMR spectra of the Dy, Tb and Tm complexes of **[LnL¹]** were measured in the absence and presence of varying Zn^{2+} concentrations in the presence of deuterated TRIS buffer at pD 7.3. In each case, the intensity of the resonance corresponding to the *tert*-butyl of the free complex decreased upon addition of ZnCl_2 . As the concentration of Zn^{2+} increased, multiple new resonances appeared making the identification of the *tert*-butyl peaks challenging. After addition of one equivalent of Zn^{2+} , all resonances were integrated and *tert*-butyl peaks were found by identifying the 9:1 ratio to other proton resonances. Trans-metallation of the lanthanide ion by the added zinc ion was not observed by NMR at this concentration, as no free ligand resonances were observed in the diamagnetic region. Upon addition of ZnCl_2 to **[DyL¹]** three new *tert*-butyl resonances appeared, each identified by integration (Figure 16).

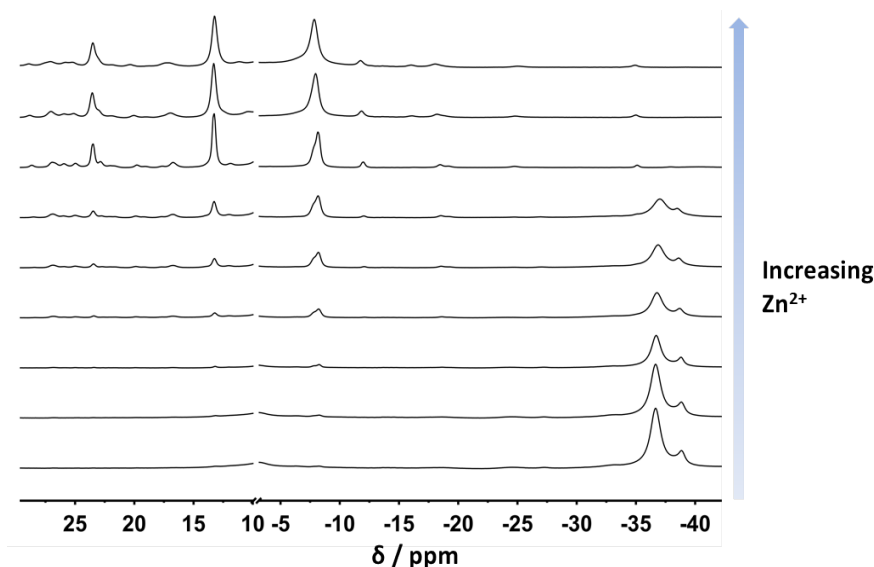


Figure 16 Stacked partial ¹H NMR spectra of the *tert*-butyl resonances of **[DyL¹]** as a function of added Zn^{2+} (D_2O , 1 M TRIS- d_{11} , pD 7.3, 11.7 T, 295 K).

A binding curve was produced by plotting the ratio of the integral of the free complex *tert*-butyl resonance and the sum of the newly formed *tert*-butyl

integrals against the number of equivalents of added Zn^{2+} (SI, Figure S5). The curve is very similar in form to that found with the luminescence titration data using **[EuL¹]**. Titrations with **[TbL¹]** and **[TmL¹]** yielded similar results (Figure 17). As with **[DyL¹]**, addition of Zn^{2+} led to the appearance of additional *tert*-butyl peaks, some of which were shifted in the opposite direction to the shift of the *tert*-butyl resonance in the starting complex.

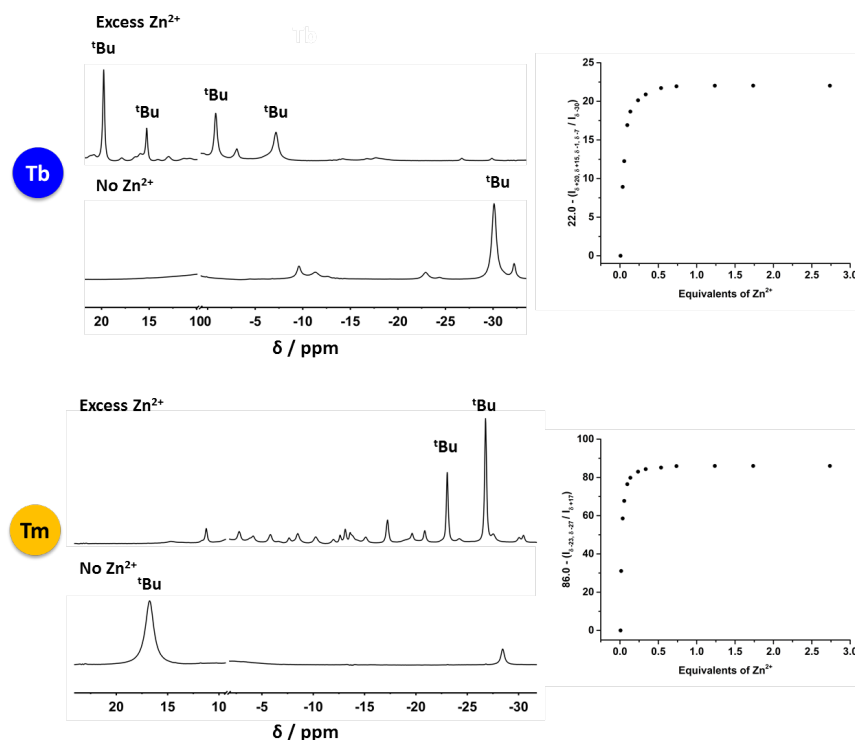





Figure 17 (Left) Stacked ¹H NMR spectra of the *tert*-butyl resonances of **[TbL¹]** (top) and **[TmL¹]** (bottom) before and after addition of excess Zn^{2+} . (Right) Ratio of the integrals of *tert*-butyl resonances of **[TbL¹]** (top) and **[TmL¹]** (bottom) as a function of the number of equivalents of added Zn^{2+} (D_2O , 1 M TRIS- d_{11} , pD 7.3, 11.7 T, 295 K).

The shift and relaxation rate data of the identified *tert*-butyl resonances for **[LnL¹]**, before and after addition of Zn^{2+} , are given in Table 4.

Table 4 Comparison of NMR properties of the *tert*-butyl resonances in [DyL¹] (*top*), [TbL¹] (*centre*) and [TmL¹] (*bottom*), with/without added Zn²⁺ (D₂O, 1 M TRIS-d₁₁, pD 7.3, 11.7 T, 295 K).

		Shift (ppm)	Linewidth (Hz)	R ₁ (Hz)	Integral
	No Zinc	-36	584	182	1
		+23	244	53	0.16
	Zinc	+13	255	55	0.31
		-8	320	21	0.52
	No Zinc	-30	280	112	1
		+20	109	44	0.33
	Zinc	+15	108	34	0.12
		-1	185	16	0.27
		-7	313	26	0.27
	No Zinc	+17	488	63	1
		-23	105	17	0.36
	Zinc	-27	110	26	0.64

Each of the longitudinal and transverse relaxation rates for the *tert*-butyl resonance in the Zn²⁺-bound complex was significantly decreased compared to that measured in the starting complex. Such a large decrease most likely arises from an increase in the distance, *r* between the paramagnetic ion and the observed resonance. Additionally, the presence of new *tert*-butyl resonances that are shifted in the *opposite* direction to [LnL¹] indicates a dramatic change in the structure of the complex upon binding Zn²⁺. Such behaviour occurs when there is change in the size and orientation of the major component of the magnetic susceptibility tensor.^{22, 27-29} The paramagnetic NMR titrimetric results are consistent with a process in which the *tert*-butyl appended pyridine moiety dissociates from the lanthanide ion following addition of Zn²⁺ ions. Similar behaviour was observed in parallel NMR studies with the diamagnetic yttrium complex, [YL¹] (see SI). No changes in the form of the proton NMR spectrum of [DyL¹] were observed when MgCl₂ or CaCl₂ were added, following addition of up to ten equivalents of salt.

Trans-metallation studies with zinc

During the NMR titration experiments a precipitate was observed to form very slowly at a Zn^{2+} equivalence greater than 1. The relatively insoluble solid obtained from the Y titration study was re-dissolved in a 50:50 mixture of acetonitrile and H_2O and electrospray mass spectral analysis of the solute revealed the presence of the protonated free Y complex, $\{[\text{YL}^1+\text{H}]^+\}$ (791.4 and 396.4), but also $\{\text{L}^1+2\text{Zn}\}^+$ and $\{\text{L}^1+2\text{Zn}+\text{H}\}^{2+}$ (833.3 and 417.3) and $\{\text{L}^1+\text{Zn}+2\text{H}\}^+$ (767.4) (SI, Fig S6). The species containing only one Zn^{2+} ion is assumed to be the 7-coordinate complex, in which Zn^{2+} has displaced Y^{3+} from the DO3A macrocycle. As Zn^{2+} is a diamagnetic ion, distinguishing between the Zn^{2+} and Y^{3+} complexes using NMR is impracticable. However, as the Zn^{2+} substituted complexes were observed as a precipitate and were found to be insoluble in most solvents, the NMR spectra acquired during the original titrations can be safely assumed to be species based on the 1:1 Y^{3+} complex, $[\text{YL}^1]$.

The time-dependent trans-metallation of DO3A-based lanthanide(III) complexes in the presence of metal cations, including Zn^{2+} , is a known process. It is normally considered to be an acid-catalysed process. The stability of various gadolinium contrast agents to trans-metallation by Zn^{2+} has been studied previously when assessing their kinetic stability.^{31,32} The longitudinal relaxation rate of water was measured in a phosphate-buffered solution in the presence of Zn^{2+} . The studies were conducted on 9-coordinate macrocyclic Gd^{3+} contrast agents based on octadentate ligands (e.g. with DOTA and HPDO3A) at pH 7 and 310 K. It was found that after 3 days, more than 98% of the original relaxivity was retained, suggesting that trans-metallation with Zn^{2+} is extremely slow. It is known that trans-metallation of lanthanide complexes occurs more quickly in 7-coordinate complexes. Similar experiments have been conducted on $[\text{GdDO3A}]$ in the presence of between 10 to 40 equivalents of Cu^{2+} .³³ Although $[\text{CuDO3A}]$ was shown to have a significantly higher stability constant ($\log K_{\text{CuL}} = 25.8$) than $[\text{GdDO3A}]$ ($\log K_{\text{GdL}} = 21.6$), the half-life of $[\text{GdDO3A}]$ in the presence of copper ions was calculated to be ~ 24 years.

Significant trans-metallation of Zn^{2+} has occurred in $[\text{YL}^1]$ at room temperature in the presence of >2 equivalents of Zn^{2+} at pH 7.3. It is unlikely that trans-metallation occurs with the free complex $[\text{YL}^1]$, as this has been shown by luminescence lifetime and NMR analysis to be at least 8-coordinate. The ease of dissociation of Y^{3+} suggests that the initial complexation of Zn^{2+} to the DPA moiety induces a conformational change that increases the susceptibility of the complex to trans-metallation. Similar behaviour was observed with the paramagnetic complexes.

Crystals of the complex $[\text{YL}^1]$ in the presence of ZnCl_2 were grown. A methanol solution of $[\text{YL}^1]$ with added ZnCl_2 . Diffusion of diethyl ether into this mixture resulted in the growth of crystals. The cationic di-zinc complex (Figure 18) crystallised as the chloride salt with hydrogen bonding to solvent methanol was observed for two of the carbonyl atoms, (CCDC 1896076); a very similar structure was found with crystals grown from an aqueous solution (CCDC 1896077).

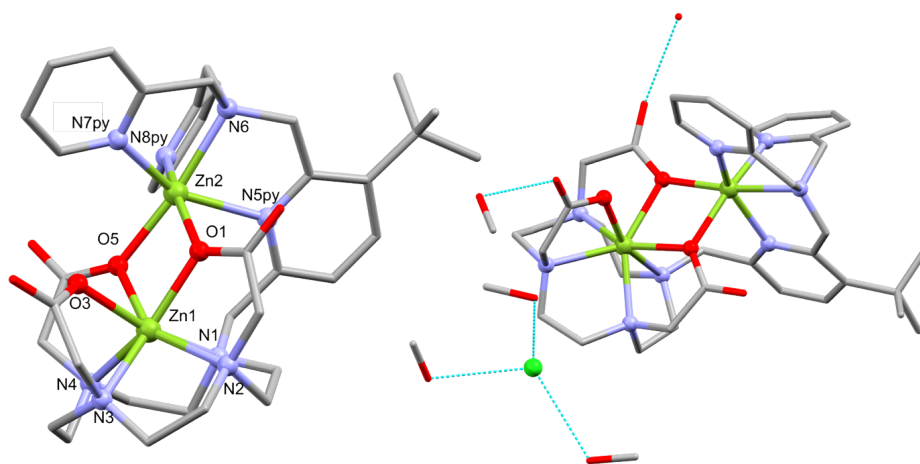


Figure 18 (left) Molecular structure of $[\text{Zn}_2\text{L}^1]$. (right) Molecular structure of $[\text{Zn}_2\text{L}^1]$ showing the chloride counter ion and hydrogen bonding to solvent methanol; H atoms are omitted for clarity, CCDC 1896076.

The two Zn^{2+} ions of $[\text{Zn}_2\text{L}^1]$ are 6- and 7- coordinate, with two of the carboxylate donors acting as bridging donors. The 7-coordinate metal (Zn1) was encapsulated within the DO3A-based macrocycle, giving an N_4O_3 coordination environment. Zinc species with such a high coordination number are relatively rare. Complexes containing a 7-coordinate Zn^{2+} ion in which the 7 donor atoms

are provided by a single polydentate ligand are even more uncommon, although there are some literature examples.³⁴⁻³⁹ Thus, the cyclen-based Zn²⁺ complex **[ZnL³]**, has been synthesised and was studied as a monomer for heterometallic coordination polymers (Figure 19).³⁹ The coordination geometry is similar to that of Zn1, however one of the O donors arises from a neutral amide carbonyl oxygen atom.

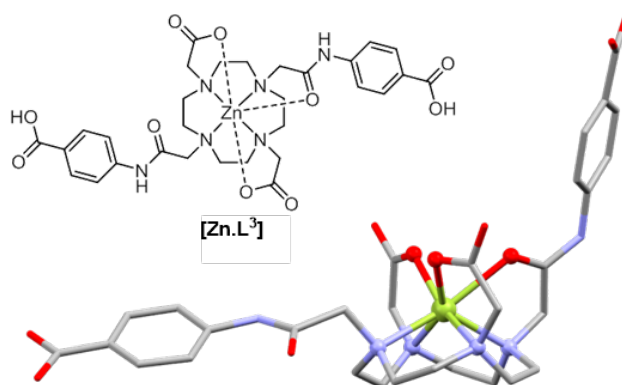


Figure 19 Molecular structure of **[ZnL³]**. H atoms are omitted for clarity.³⁸ CCDC: 1443839 / MABVET.

The 6-coordinate Zn²⁺ ion (Zn2) was ligated by the four nitrogen donors of the tripicolyl moiety and the two bridging carboxylates, in a distorted octahedral (N₄O₂) geometry. The geometry of Zn2 is similar to that of the dimeric Zn-TPA complex **[Zn₂(TPA)₂(OH)₂]²⁺** (Figure 20),⁴⁰ in which both Zn²⁺ ions are ligated in a distorted octahedral geometry by the 4 neutral nitrogen donors of the TPA ligand and two bridging O donors. In this case the bridging O donors are hydroxide groups; carboxylate bridges (μ -O_{carboxylate}) in di-zinc species are also known.⁴¹⁻⁴³ The Zn-Zn distance of **[Zn₂L¹]** was found to be 3.36 Å which is comparable to those reported in a small set of similar zinc complexes with (μ -O_{carboxylate})₂ bridges (3.11 – 3.50 Å).⁴⁰

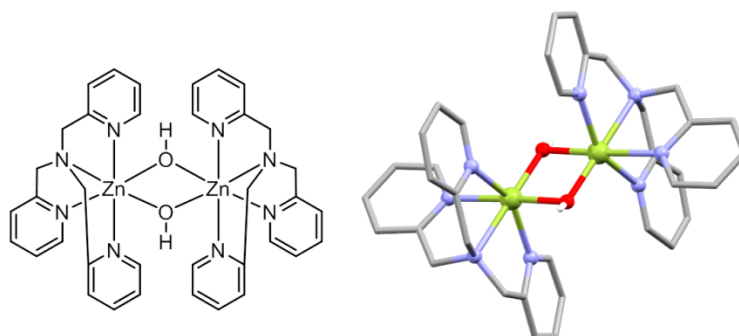


Figure 20 Molecular structure of $[\text{Zn}_2(\text{TPA})_2(\text{OH})_2]^{2+}$. ³⁹ H atoms of the TPA ligand are omitted for clarity. CCDC: 1230684 / PEMBIS.

As the ionic radius of Zn^{2+} is much smaller than that of Dy^{3+} , the metal-donor bond distances to the transition metal are decreased from those seen in $[\text{DyL}^1]$ (Table 5).

Table 5 Bond distances (\AA) for Zn1 (*left*) and Zn2 (*right*) in $[\text{Zn}_2\text{L}^1]^+$.

bond	bond distance (\AA)
Zn1-N1	2.418(5)
Zn1-N2	2.237(4)
Zn1-N3	2.342(5)
Zn1-N4	2.212(5)
Zn1-O1	2.080(3)
Zn1-O3	2.123(4)
Zn1-O5	2.244(3)

bond	bond distance (\AA)
Zn2-N5py	2.236(4)
Zn2-N6	2.183(4)
Zn2-N7py	2.120(4)
Zn2-N8py	2.179(5)
Zn2-O1	2.125(3)
Zn2-O5	2.060(3)

Summary and Conclusions

An NMR Zn^{2+} -selective probe, $[\text{LnL}^1]$, has been synthesised and characterised. It is based on a DO3A macrocycle bearing a pendant pyridine ring containing both a *tert*-butyl NMR reporter group and a DPA moiety. The tripicolyl amine Zn^{2+} moiety was synthesised using a ten-step linear synthesis, including a regioselective reduction step, with the aid of simple protecting group chemistry. Solid-state structural analysis showed that the Dy complex was nine-coordinate, with the amine nitrogen atom of the DPA moiety completing the coordination in which there is a long, axial bond to the lanthanide ion. At high temperature or

low pH this bond was in solvent exchange or was cleaved, as observed from lifetime measurements of the Eu^{3+} and Tb^{3+} complexes and the diamagnetic and paramagnetic NMR spectral behaviour of the Y^{3+} and Dy^{3+} complexes. The $\text{p}K_{\text{a}}$ value of the complex was measured to be 5.70 by luminescence methods. This value is low enough that changes in pH within a biological range of 6.5-7.5 will have minimal impact on the behaviour of the complex.

The *tert*-butyl resonance of the Dy, Tb and Tm complexes was shifted well beyond the diamagnetic region, in principle allowing the resonance to be imaged against zero background. The shift and relaxation properties of these systems have been investigated at different temperatures and magnetic fields. Relatively fast longitudinal relaxation rates at low fields allow faster spectral acquisition.

The binding to Zn^{2+} has been probed using both luminescence (Eu) and NMR (Y, Dy, Tb, Tm, Er) studies revealing a high affinity. Large changes were observed in emission and NMR properties of the complexes, consistent with a predominant 1:1 binding stoichiometry, suggesting a decrease in the coordination number of the lanthanide ion. Mass spectrometry studies provided further proof of 1:1 speciation. Selectivity was demonstrated for Zn^{2+} over Ca^{2+} and Mg^{2+} and binding reversibility was shown through competitive titrations with EDTA and DTPA. The affinity of the complex to Zn^{2+} could be adapted by modification of the chelating group. Removal of one of the pyridines of the DPA moiety could reduce the Zn^{2+} binding strength but the replacement chelating moiety must be chosen carefully, to avoid any loss of binding selectivity.

At higher concentrations of Zn^{2+} and with time, trans-metallation was observed in which the lanthanide is replaced to form a novel di-zinc species. Trans-metallation of DO3A-based lanthanide complexes is unprecedented at this pH. X-ray crystallographic analysis elucidated the solid-state structure of the di-zinc species. One Zn^{2+} ion was found to be 7-coordinate, an unusually high, although not unique, coordination number. Two carboxylate groups of the DO3A macrocycle were found to bridge the Zn^{2+} ions. The kinetic stability of the complex with respect to trans-metallation within biological media must be explored in more detail.

Further *in vitro* work to investigate any potential interactions with proteins is also required to ensure that binding to Zn^{2+} would be unperturbed *in vivo*. Additional titrations in serum would allow for the creation of more relevant calibration curves and phantom imaging studies using a preclinical MRI scanner could then be used to demonstrate the feasibility of the *in vivo* measurement of Zn^{2+} , in areas where the local concentration is known to be high, such as the prostate gland.

Acknowledgements We thank EPSRC for partial studentship support, Dr Dmitry Yufit for help with the X-ray crystallography and Drs Alan M Kenwright and Juan A Aguilar for help with NMR experiments. The authors declare no conflicts of interest.

References

- 1 a) C. J. Frederickson, J. Y. Koh and A. I. Bush, *Nat. Rev. Neurosci.*, **2005**, *6*, 449–462; b) S. T. Lo, A. F. Martins, V. C. Jordan and A. D. Sherry, *Isr. J. Chem.* **2017**, *57*, 854–861; L. C. Costello, and R. B. Franklin, *Mol. Cancer* **2006**, *5*, 59–63.
- 2 P. Jiang and Z. Guo, *Coord. Chem. Rev.*, **2004**, *248*, 205–229.
- 3 K. P. Carter, A. M. Young and A. E. Palmer, *Chem. Rev.*, **2014**, *114*, 4564–4601.
- 4 G. K. Walkup, S. C. Burdette, S. J. Lippard and R. Y. Tsien, *J. Am. Chem. Soc.*, **2000**, *122*, 5644–5645.
- 5 a) D. W. Gruenwedel, *Inorg. Chem.*, **1968**, *7*, 495–501; b) G. Anderegg and F. Wenk, *Helv. Chim. Acta*, **1967**, *50*, 2330; c) B. Mandel, C. Mariconi, B. E. Douglas, *Inorg. Chem.* **1988**, *27*, 2990; d) Y-H. Chiu and J. W. Canary, *Inorg. Chem.* **2003**, *42*, 5107–5116.
- 6 G. Anderegg and E. Hubmann, *Helv. Chim. Acta*, **1977**, *60*, 123–140.
- 7 C. S. Bonnet and É. Tóth, *Future Med. Chem.*, **2010**, *2*, 367–384.
- 8 E. L. Que and C. J. Chang, *Chem. Soc. Rev.*, **2010**, *39*, 51–60.
- 9 K. Hanaoka, K. Kikuchi, Y. Urano and T. Nagano, *J. Chem. Soc. Perkin Trans. 2*, **2001**, *25*, 1840–1843.

- 10 K. Hanaoka, K. Kikuchi, Y. Urano, M. Narazaki, T. Yokawa, S. Sakamoto, K. Yamaguchi and T. Nagano, *Chem. Biol.*, **2002**, *9*, 1027–1032.
- 11 R. Trokowski, J. Ren, F. K. Kálmán and A. D. Sherry, *Angew. Chem. Int. Ed.*, **2005**, *44*, 6920–6923.
- 12 A. C. Esqueda, J. A. López, G. Andreu-de-Riquer, J. C. Alvarado-Monzón, J. Ratnakar, A. J. M. Lubag, A. D. Sherry and L. M. De León-Rodríguez, *J. Am. Chem. Soc.*, **2009**, *131*, 11387–11391.
- 13 A. J. M. Lubag, L. M. De Leon-Rodriguez, S. C. Burgess and A. D. Sherry, *Proc. Natl. Acad. Sci.*, **2011**, *108*, 18400–18405.
- 14 M. V. Clavijo Jordan, S.-T. Lo, S. Chen, C. Preihs, S. Chirayil, S. Zhang, P. Kapur, W.-H. Li, L. M. De Leon-Rodriguez, A. J. M. Lubag, N. M. Rofsky and A. D. Sherry, *Proc. Natl. Acad. Sci.*, **2016**, *113*, 5464–5471.
- 15 J. L. Major, G. Parigi, C. Luchinat and T. J. Meade, *Proc. Natl. Acad. Sci.*, **2007**, *104*, 13881–13886.
- 16 J. L. Major, R. M. Boiteau and T. J. Meade, *Inorg. Chem.*, **2008**, *47*, 10788–10795.
- 17 X.-A. Zhang, K. S. Lovejoy, A. Jasanoff and S. J. Lippard, *Proc. Natl. Acad. Sci.*, **2007**, *104*, 10780–5.
- 18 T. Lee, X. Zhang, S. Dhar, H. Faas, S. J. Lippard and A. Jasanoff, *Chem. Biol.*, **2010**, *17*, 665–673.
- 19 a) K-L. N. A. Finney, A. C. Harnden, N. J. Rogers, P. K. Senanayake, A. M. Blamire, D. O'Hogain and D. Parker, *Chem. Eur. J.* **2017**, *23*, 7976–7989; b) A. C. Harnden, D. Parker, and N. J. Rogers, *Coord. Chem. Rev.* **2019**, *383*, 30–42.
- 20 P. K. Senanayake, N. J. Rogers, P. Harvey, K-L. N. A. Finney, A. M. Funk, D. Parker, J. I. Wilson, R. Maxwell, A. M. Blamire, *Magn. Reson. Med.* **2017**, *77*, 1307–1317.
- 21 a) D. Coman, R. A. de Graaf, D. L. Rothman, F. Hyder, *NMR Biomed.* **2013**, *26*, 1589–1593; b) Y. Huang, D. Coman, P. Herman, J. U. Rao, S. Maritim, F. Hyder, *NMR Biomed.* **2016**, *29*, 1364–1372.
- 22 S. J. A. Pope and R. H. Laye, *Dalton Trans.*, **2006**, *44*, 3108.

23. A. Beeby, I. M. Clarkson, R. S. Dickins, S. Faulkner, D. Parker, L. Royle, A. S. de Sousa, J. A. G. Williams and M. Woods, *J. Chem. Soc. Perkin Trans. 2*, 1999, **2**, 493–504.
24. K. Mason, N. J. Rogers, E. A. Suturina, I. Kuprov, J. A. Aguilar, A. S. Batsanov, D. S. Yufit and D. Parker, *Inorg. Chem.* **2017**, *56*, 4028-4038.
25. A. Krezel and W. Bal, *J. Inorg. Biochem.*, **2004**, *98*, 161-166.
26. D. Parker, R. S. Dickins, H. Puschmann, C. A. Crossland and J. A. K. Howard, *Chem. Rev.* **2002**, *102*, 1977-2010.
27. R. S. Dickins, D. Parker, J. I. Bruce and D. J. Tozer, *Dalton Trans.*, 2003, 1264–1271.
28. O. A. Blackburn, N. F. Chilton, K. Keller, C. E. Tait, W. K. Myers, E. J. L. McInnes, A. M. Kenwright, P. D. Beer, C. R. Timmel and S. Faulkner, *Angew. Chem. Int. Ed.*, 2015, **54**, 10783–10786.
29. E. A. Suturina, K. Mason, C. F. G. C. Geraldés, I. Kuprov and D. Parker, *Angew. Chem. Int. Ed.* **2017**, *56*, 12215-12218.
30. S. Shuvaev, M. A. Fox and D. Parker, *Angew. Chem. Int. Ed.*, 2018, **57**, 7488–7492.
31. S. Laurent, L. Vander Elst, F. Copoix and R. N. Muller, *Invest. Radiol.*, 2001, **36**, 115–122.
32. S. Laurent, L. Vander Elst and R. N. Muller, *Contrast Media Mol. Imaging*, 2006, **1**, 128–137.
33. A. Takács, R. Napolitano, M. Purgel, A. C. Bényei, L. Zékány, E. Brücher, I. Tóth, Z. Baranyai and S. Aime, *Inorg. Chem.*, 2014, **53**, 2858–2872.
34. G. de Martino Norante, M. Di Vaira, F. Mani, S. Mazzi and P. Stoppioni, *Inorg. Chem.*, 1990, **29**, 2822–2829.
35. S. Aoki, H. Kawatani, T. Goto, E. Kimura and M. Shiro, *J. Am. Chem. Soc.*, 2001, **123**, 1123–1132.
36. H. Keypour, H. Khanmohammadi, K. P. Wainwright and M. R. Taylor, *Inorg. Chim. Acta*, 2003, **355**, 286–291.
37. L. Vaiana, C. Platas-Iglesias, D. Esteban-Gómez, F. Avecilla, A. De Blas and T. Rodríguez-Blas, *Eur. J. Inorg. Chem.*, 2007, 1874–1883.
38. L. Vaiana, M. Regueiro-Figueroa, M. Mato-Iglesias, C. Platas-Iglesias, D. Esteban-

- Gómez, A. De Blas and T. Rodríguez-Bias, *Inorg. Chem.*, 2007, **46**, 8271–8282.
- 39 J. Aríñez-Soriano, J. Albalad, J. Pérez-Carvajal, I. Imaz, F. Busqué, J. Juanhuix and D. Maspoch, *CrystEngComm*, 2016, **18**, 4196–4204.
- 40 N. N. Murthy and K. D. Karlin, *J. Chem. Soc. Chem. Commun.*, 1993, 1236.
- 41 J. M. González Pérez, J. Niclós Gutiérrez, D. Nguyen-Huy, B. Viossat, A. Busnot and M. Wintenberger, *Inorg. Chim. Acta*, 1991, **184**, 243–249.
- 42 A. Gorrane, A. Pastor, E. Álvarez, C. Mealli, A. Ienco and A. Galindo, *Inorg. Chem. Commun.*, 2006, **9**, 160–163.
- 43 S. Shit, A. Sasmal, P. Dhal, C. Rizzoli and S. Mitra, *J. Mol. Struct.*, 2016, **1108**, 475–481.

Graphic for TOC

